Dynamic phosphorylation of Hcm1 promotes fitness in chronic stress

Michelle M. Conti[1], Jillian P. Bail[1], Rui Li[1], Lihua Julie Zhu[1,2,3], Jennifer A. Benanti[1,*]

[1]Department of Molecular, Cell and Cancer Biology, University of Massachusetts Chan Medical School, Worcester, MA 01605.

[2]Department of Genomics and Computational Biology, University of Massachusetts Chan Medical School, Worcester MA 01605.

[3]Program in Molecular Medicine, University of Massachusetts Chan Medical School, Worcester MA 01605.

*Correspondence: jennifer.benanti@umassmed.edu

Summary

Cell survival depends upon the ability to adapt to changing environments. Environmental stressors trigger an acute stress response program that rewires cell physiology, downregulates proliferation genes and pauses the cell cycle until the cell adapts. Here, we show that dynamic phosphorylation of the yeast cell cycle-regulatory transcription factor Hcm1 is required to maintain fitness in chronic stress. Hcm1 is activated by cyclin dependent kinase (CDK) and inactivated by the phosphatase calcineurin (CN) in response to stressors that signal through increases in cytosolic Ca^{2+}. Expression of a constitutively active, phosphomimetic Hcm1 mutant reduces fitness in stress, suggesting Hcm1 inactivation is required. However, a comprehensive analysis of Hcm1 phosphomutants revealed that Hcm1 activity is also important to survive stress, demonstrating that Hcm1 activity must be toggled on and off to promote gene expression and fitness. These results suggest that dynamic control of cell cycle regulators is critical for survival in stressful environments.

Introduction

Cells are continuously exposed to stressors in the environment and must adapt to these challenges to survive and proliferate. Adaptation not only protects healthy cells from death, but conversely, it can promote the development of disease. For instance, cancer cells must adapt to stressful environments when they metastasize to distant sites[1], and fungal pathogens rely upon stress response pathways for survival within the host[2]. Despite the importance of this process, the long-term changes that cells must undergo to maintain fitness and proliferation when faced with chronic stress are poorly understood.

The acute stress response, which occurs immediately following exposure to an environmental stressor, is conserved from yeast to humans and includes a downregulation of protein synthesis and an upregulation of stress response genes[3,4]. In addition to these changes that impact cell physiology, cell cycle-regulatory genes are downregulated, and cells undergo a

27 transient cell cycle arrest[5,6]. After cells adapt to the new environment, the acute stress response
28 is resolved and cells resume proliferation in the new environment, albeit at a reduced rate[7]. It is
29 thought that it is important to pause cell division while cells undergo adaptation to promote long-
30 term survival[8,9], however this has not been examined for most stressors.

31 Some stressors signal through an increase in cytosolic Ca^{2+} and coordinate the stress
32 response program and cell cycle changes by activating the conserved Ca^{2+}-activated
33 phosphatase calcineurin (CN)[10,11]. CN activation leads to a decrease in expression of cell cycle-
34 regulatory genes and controls the length of cell cycle arrest, in combination with the stress
35 activated MAPK Hog1/p38[12]. One direct target of CN in budding yeast is the S-phase transcription
36 factor (TF) Hcm1[13]. Hcm1 is a forkhead family transcriptional activator which, like it's human
37 homolog FoxM1, plays a crucial role in maintaining genome stability[14,15]. Hcm1 regulates
38 expression of key cell cycle genes including histone genes, downstream cell cycle-regulatory TFs,
39 and genes that regulate mitotic spindle function. As cells progress through the cell cycle, Hcm1 is
40 activated by multisite phosphorylation by cyclin dependent kinase (CDK)[16]. CDK phosphorylates
41 eight sites in the Hcm1 transactivation domain (TAD) to stimulate its activity and a three site
42 phosphodegron in the N-terminus to trigger proteasomal degradation. Immediately following
43 exposure to $CaCl_2$ or LiCl stress, two stressors that activate CN, CDK activity decreases, the
44 activating phosphates on Hcm1 are specifically removed by CN, and expression of Hcm1 target
45 genes decreases[12,13,17]. Whether or not Hcm1 inactivation is critical for cells to adapt and survive
46 in the face of chronic stress is unknown.

47 Mutations within the Hcm1 TAD have been used to study the consequences of
48 phosphorylation. Phosphomimetic mutations at all CDK phosphosites in the TAD generate a
49 constitutively active protein that leads to increased expression of Hcm1 target genes[16]. In normal
50 growth conditions this mutant provides a fitness advantage to cells, rendering them more fit than
51 wild type (WT)[13,18]. This is a surprising result because advantageous mutations are expected to
52 be selected for during evolution. However, the fact that activating phosphates are removed by CN

53 when cells are faced with stress suggests that dephosphorylation and inactivation of Hcm1 may
54 be necessary for cells to survive in stressful environments.

55 Here, we investigated this possibility and found that cells expressing a constitutively active,
56 phosphomimetic Hcm1 mutant lose their fitness advantage when exposed to LiCl stress for
57 several days. To determine the optimal level of Hcm1 activity for fitness in this environment, we
58 screened a collection of Hcm1 mutants that encompass all possible combinations of non-
59 phosphorylatable and phosphomimetic mutations in the TAD, representing the entire spectrum of
60 possible activity levels. Surprisingly, this screen revealed that almost all mutants were less fit
61 when growing in stress compared to stress-free conditions. Moreover, Cks1-docking sites that
62 stimulate Hcm1 activity by promoting processive phosphorylation by CDK became more important
63 for fitness when cells were grown in chronic stress. Finally, mutants that have increased Hcm1
64 activity because proteasomal degradation is blocked, but retain dynamic phosphoregulation of
65 the TAD, were more fit than WT cells in chronic stress. These results demonstrate that simple
66 Hcm1 inactivation is not the mechanism by which cells survive in chronic stress; instead, dynamic
67 regulation of the Hcm1 activity – obtained through a combination of phosphorylation by CDK and
68 dephosphorylation by CN – is critical to maintain fitness.

69

70 **Results**

71

72 **Expression of a phosphomimetic Hcm1 mutant decreases fitness in LiCl stress**

73 CDK phosphorylates eight sites in the Hcm1 TAD to activate the protein during an unperturbed
74 cell cycle. When cells are exposed to a CN-activating stressor such as $CaCl_2$ or LiCl, these
75 phosphates are removed by the phosphatase CN[13,18] (Figure 1A). This dephosphorylation occurs
76 rapidly after exposure to LiCl[13] and, notably, Hcm1 remains in a hypophosphorylated state after
77 cells adapt to LiCl stress and resume cycling (Figure 1B). To determine if dephosphorylation of
78 Hcm1 is necessary for cells to survive when faced with chronic LiCl stress, we utilized a

79 constitutively active phosphomimetic Hcm1 mutant, Hcm1-8E, in which each CDK site in the TAD
80 is mutated to two glutamic acids (S/T-P to E-E) to mimic the charge of a phosphate[16,18]. The Hcm1-
81 8E protein is more active than WT Hcm1 and, as a result, confers a fitness advantage to cells in
82 a competitive growth assay in optimal growth conditions that lack environmental stressors. To
83 determine the consequence of elevated Hcm1 activity in stress, we compared the fitness of cells
84 expressing Hcm1-8E to cells expressing WT Hcm1, in the presence or absence of LiCl (Figure
85 1C-1D). As previously shown, *hcm1-8E* cells exhibited a fitness benefit in the absence of stress
86 (Figure 1C). However, *hcm1-8E* cells lost their fitness advantage and displayed a modest fitness
87 defect when cultured in medium containing LiCl (Figure 1D), supporting the possibility that cells
88 need to inactivate Hcm1 to survive in the presence of chronic LiCl stress.
89
90 **Hcm1 mutants with fixed phosphorylation states are less fit in LiCl stress**
91 Hcm1 retains some phosphorylation when cells are grown for three days in LiCl (Figure 1B),
92 suggesting that some activity may remain, and that a reduced level of Hcm1 activity might be
93 optimal in stress. To test this hypothesis, we employed Phosphosite Scanning, a recently
94 developed screening approach that can simultaneously determine the effects of hundreds of
95 phosphosite mutations on cellular fitness[18]. In this approach, a collection of strains expressing
96 different phosphomutant proteins are pooled and passaged together. The abundance of each
97 mutant in the population is followed over time by deep sequencing and a selection coefficient is
98 calculated, based on the change in abundance of each mutant over time relative to WT. Screening
99 libraries of mutants with all possible combinations of unphosphorylatable and phosophomimetic
100 mutations enables the determination of the contribution of each individual phosphosite to a fitness
101 phenotype.
102 To determine how different levels of Hcm1 activity impact fitness in stress, we performed
103 Phosphosite Scanning screens with a collection of mutants in which each CDK phosphosite (S/T-
104 P) in the TAD is mutated to an unphosphorylatable alanine (A-P) or two glutamic acids (E-E), in

105 all possible combinations (A/E library, Figure S1A)[18]. In unstressed growth conditions, fitness
106 values conferred by these Hcm1 mutants are highly correlated with the activity of each mutant
107 and this collection of mutants represents the entire continuum of possible Hcm1 activities, from
108 the completely inactive Hcm1-8A mutant (with all phosphosites mutated to A-P) to the Hcm1-8E
109 mutant that has increased activity relative to WT[18]. To determine how each Hcm1 mutant impacts
110 fitness in stress, these mutants were simultaneously screened in control and LiCl containing
111 media (Figure 2A).

112 First, we examined how overall fitness was impacted when cells were growing in stress.
113 Selection coefficients of each mutant in LiCl-containing medium were directly compared with
114 those from control medium (Figure 2B). Surprisingly, although there was a strong correlation
115 between selection coefficients in the two environments, almost all mutants were less fit in LiCl
116 than control conditions. This effect was most severe for mutants with greatest number of
117 phosphomimetic (activating) mutations (Figure 2C), whereas mutants that had two or fewer
118 phosphomimetic mutations were most similar between control and LiCl media. Notably, although
119 the *hcm1-8E* mutant displayed a modest fitness defect in pairwise competition assays carried out
120 in LiCl (Figure 1D), it had a slight fitness advantage in pooled screens. This observation is likely
121 due to technical differences in the experimental approach, and consistent with previous findings
122 that pooled screens result in slightly higher selection coefficients than pairwise competition
123 assays[18]. However, the *hcm1-8E* mutant fitness advantage was modest in pooled LiCl screens
124 and decreased in LiCl compared to control conditions (Figure 2C, mutant with eight E
125 substitutions). These data demonstrate that Hcm1 activity is required for fitness in stress, however
126 the most highly active mutants exhibit large reductions in fitness compared to control growth
127 conditions.

128 Next, we wanted to determine how individual TAD phosphosites impact cellular fitness in
129 LiCl stress. To do this, we compared the selection coefficients of all mutants that had either a non-
130 phosphorylatable alanine (A) or two glutamic acids (E) at each site (Figure 2D, 2E). In both control

131 and LiCl conditions, a phosphomimetic mutation at any site increased fitness relative to an alanine
132 substitution at the same site. Notably, mutations at sites T460 and S471 had the greatest effect
133 on fitness in both conditions, consistent with previous measurements in the absence of stress[18].
134 Together, these data show that when phosphorylation patterns of Hcm1 are fixed because all sites
135 are changed to either phosphodeficient or phosphomimetic amino acids, the fitness of almost all
136 mutants is decreased in stress. This raises the possibility that it is not inactivation of Hcm1 that is
137 important for cells to maintain fitness in stress, but rather dynamic regulation conferred by
138 phosphorylation and dephosphorylation of the TAD.
139
140 **Elevated importance of processive Hcm1 phosphorylation in stress**
141 To investigate the importance of dynamic phosphorylation of Hcm1 in stress, we used
142 Phosphosite Scanning to screen libraries of mutants that include WT phosphosites in combination
143 with phosphodeficient or phosphomimetic mutations. In contrast to the A/E library, in which all
144 phosphosites are fixed, the inclusion of WT sites allows some phosphorylation by CDK during the
145 experiment and can reveal how a fixed phosphorylation state at one site influences
146 phosphorylation at other sites[18]. We screened two collections of mutants: one in which all sites
147 are either WT or a non-phosphorylatable alanine (WT/A library, Figure S1B); and one in which all
148 sites are either WT or phosphomimetic (WT/E library, Figure S1C)[18]. The fitness of all mutants
149 was compared between control conditions and LiCl conditions, as described above.
150 First, we asked whether all eight sites in the TAD contribute to fitness in LiCl stress, by
151 analyzing the results from the WT/A library screen. Similar to the A/E screen, selection coefficients
152 for all mutants were correlated between control and LiCl stress, however all scores were reduced
153 in LiCl compared to control (Figure S2A). Moreover, alanine substitutions in an otherwise WT
154 background reduced fitness to a greater extent than observed when the same alanine
155 substitutions were included an otherwise phosphomimetic background (compare Figure S2B with
156 Figure 2C). This observation is consistent with a previous discovery that CDK relies upon the

157 phosphoadapter subunit Cks1 to promote phosphorylation of critical regulatory sites in the Hcm1
158 TAD[18]. Cks1 can only bind to phosphothreonine[19,20], so alanine substitutions reduce activity in two
159 ways: first, activity is directly reduced because alanines cannot be phosphorylated and provide
160 the charge conferred by a phosphate and second, activity is indirectly decreased because
161 alanines cannot interact with Cks1 and thereby reduce phosphorylation of more C-terminal WT
162 sites in the domain. Despite the decreased fitness of all mutants in the WT/A library, fitness
163 generally increased with the number of WT sites in any given mutant (Figure S2B), and a WT site
164 was more advantageous than an alanine at each position (Figure S2C, S2D), in both control and
165 LiCl conditions. These results support the conclusion that phosphorylation at each site contributes
166 to Hcm1 activity in both control and stress conditions.

167 We further explored the contribution of Cks1 priming sites to fitness in stress by screening
168 the WT/E library (Figure S1C). Like alanine mutations, phosphomimetic (E-E) mutations cannot
169 serve as Cks1 priming sites. Because of this, E-E substitutions effectively behave as separation
170 of function mutations: they contribute to Hcm1 activation because they are charged, but are
171 unable to act as Cks1 priming sites, so they impair phosphorylation of more C-terminal WT sites
172 in the TAD. The cumulative effect of these mutations is evident when comparing selection
173 coefficients of WT/E mutants in control and LiCl conditions (Figure 3A). Whereas most mutants
174 in this collection are more fit than WT in control conditions, the majority of mutants become less
175 fit than WT in stress (Figure 3A, lower right quadrant). The subset of mutants that remained more
176 fit than WT in stress included most mutants that have phosphomimetic mutations at T460 and
177 S471, likely because this group of mutants does not depend on Cks1 priming to facilitate the
178 phosphorylation of these two sites that have the greatest impact on Hcm1 activity (Figure 2D).
179 Notably, in the WT/E library, fitness did not increase with the number of phosphomimetic mutations
180 when cells were growing in LiCl (Figure 3B), suggesting that priming by Cks1 is of increased
181 importance when cells are growing in stress.

182 To further investigate the need for Cks1 priming, we analyzed the fitness of
183 phosphomutants based on their genotype at each site. If a phosphomimetic mutation has a
184 negative effect and confers a reduced selection coefficient compared to the WT CDK site, it
185 suggests that position functions as a priming site[18]. For example, in control media mutants that
186 are phosphomimetic at site 428 are less fit than mutants that are WT at the same site, indicating
187 that site 428 is a Cks1 priming site (Figure 3C)[18] .Notably, this deleterious fitness effect was
188 amplified in LiCl stress, and there was a similar reduction in fitness among mutants that are
189 phosphomimetic at site 440 (Figure 3D). Interestingly, mutants that were phosphomimetic at two
190 additional sites, 479 and 486, also showed a reduction in fitness relative to mutants that are WT
191 at the same sites in LiCl. Since these phosphomimetic mutations improved or had little effect on
192 fitness in control conditions (Figure 3C), it suggests that these may be additional Cks1 priming
193 sites within the Hcm1 TAD that only become important for fitness in stress. In fact, mutants with
194 phosphomimetic mutations at either T428 and T440 or T479 and T468 displayed significantly
195 reduced fitness in stress compared to mutants with WT sites, despite equivalent fitness in control
196 conditions (Figure 3E, 3F). The importance of Cks1-dependent priming supports the conclusion
197 that dynamic phosphorylation of the Hcm1 TAD is critical for fitness when cells are challenged
198 with LiCl stress.
199
200 **Dynamic phosphorylation of the Hcm1 TAD is required for fitness in stress**
201 If the *hcm1-8E* mutant is less fit in stress because its phosphorylation cannot be dynamically
202 regulated, and not because it has increased activity, then an alternative mutant in which activity
203 is increased by a different mechanism might not exhibit reduced fitness in stress. To test this
204 possibility, we examined the fitness of *hcm1-3N* mutant cells. Hcm1-3N contains three alanine
205 substitutions in the N-terminal phosphodegron that prevent proteasomal degradation and stabilize
206 the protein, thereby increasing Hcm1 activity without perturbing TAD phosphorylation dynamics
207 (Figure 4A)[16]. Cells expressing Hcm1-3N exhibit similar increases in fitness as Hcm1-8E

208 expressing cells, compared to WT, in the absence of stress (Figure 4B, 1C, 4F)[13,18]. Importantly,
209 the Hcm1-3N mutant contains a WT TAD, so phosphorylation is reduced in chronic stress, despite
210 increased Hcm1 protein levels (Figure S3A, S3B). If it is dynamic regulation of Hcm1 that is
211 important for fitness in stress, *hcm1-3N* cells should differ from *hcm1-8E* and retain their fitness
212 advantage.

213 To test this hypothesis, pairwise competition assays were carried out between *hcm1-3N*
214 and WT cells in control and LiCl containing medium. Consistent with previous observations, *hcm1-*
215 *3N* cells were more fit than WT cells in control conditions (Figure 4B, 4F). Notably, in contrast to
216 the decreased fitness observed in *hcm1-8E* cells (Figure 1D, 4F), the fitness benefit in *hcm1-3N*
217 cells was enhanced when cells were challenged with LiCl stress (Figure 4C, 4F). To compare
218 these effects directly, these two sets of mutations were combined to generate a stable,
219 constitutively active mutant (*hcm1-3N8E*, Figure 4A). In a pairwise competition assay, *hcm1-3N8E*
220 cells had similar fitness as *hcm1-3N* cells in control conditions (Figure 4D), as previously
221 reported[18]. However, *hcm1-3N8E* cells were less fit than *hcm1-3N* in LiCl stress (Figure 4E).
222 Therefore, preventing dynamic phosphorylation reverses the fitness benefit provided by increased
223 Hcm1 expression in stress.

224 When cells are continuously exposed to a CN-activating stress, cells experience bursts in
225 cytosolic Ca^{2+}, followed by pulses of CN activity[21,22]. This suggests that Hcm1 may undergo pulses
226 of inactivation in chronic stress, which could then be reversed by CDK activity. For some TFs,
227 increasing the frequency of activation results in a greater induction of target gene expression,
228 compared to increasing the amplitude of TF activity[23,24]. Therefore, we considered that Hcm1 may
229 undergo pulses of activity in stress, through modulation of phosphorylation, which in turn could
230 impact the expression of its target genes. If so, *hcm1-8E* cells may be unable to activate target
231 genes to the same extent as *hcm1-3N* when exposed to stress. To test this hypothesis, cells
232 expressing WT Hcm1, Hcm1-3N or Hcm1-8E were grown in control medium or LiCl for 40 hours
233 and Hcm1 target gene expression was quantified by RNA sequencing. Hcm1 only activates target

234 gene expression during S-phase. Consequently, because the experiment was performed in
235 asynchronous cultures, where only ~16% of cells are in S-phase (Figure S3C), we observed
236 modest fold change differences between wild type and mutant strains for individual Hcm1 target
237 genes (Dataset S2). For this reason, we used Gene Set Enrichment Analysis (GSEA) to examine
238 changes in expression of Hcm1 target genes as a group. GSEA revealed that Hcm1 targets were
239 collectively expressed at elevated levels in both *hcm1-3N* and *hcm1-8E* mutants compared to WT
240 in unstressed conditions, confirming that the two mutants exhibit a similar increase in activity
241 (Figure 4G, a negative normalized enrichment score (NES) indicates lower expression in WT
242 compared to mutant). However, when cells were grown in LiCl, Hcm1 target genes increased in
243 expression in *hcm1-3N* cells, but not in *hcm1-8E* cells. Moreover, target genes were more highly
244 expressed in *hcm1-3N* cells than *hcm1-8E* cells when they were directly compared (Figure 4G).
245 These results demonstrate that dynamic phosphorylation of Hcm1 in stress increases expression
246 of Hcm1 target genes and suggests that expression of these genes promotes fitness in stress.
247

248 **Discussion**

249 Immediately upon exposure to an environmental stressor, cells rewire many cellular pathways to
250 promote stress resistance and long-term survival. A conserved feature of this acute response is
251 the inactivation of cell cycle-regulatory TFs and downregulation of their target genes. Although
252 cell cycle arrest is not required for the execution of the acute stress response[9], it is possible that
253 arrest and/or downregulation of cell cycle-regulatory genes is important for adaptation and
254 survival after cells resume proliferation in the new environment. In support of this possibility, we
255 found that expression of the Hcm1-8E phosphomimetic mutant, which cannot be
256 dephosphorylated and inactivated, reduces fitness in chronic LiCl stress (Figure 1D). However,
257 several pieces of evidence argue that simple Hcm1 inactivation does not promote fitness in stress,
258 but rather its phosphorylation must be dynamically regulated to activate target gene expression
259 and ensure fitness. First, almost all Hcm1 phosphosite mutants that retain activity but have fixed

260 phosphorylation states are less fit in LiCl than control conditions (Figure 2B). This includes
261 mutants that have WT-like activity, as well as those that have increased activity compared to WT.
262 Second, TP motifs that function as Cks1 priming sites to promote processive phosphorylation by
263 CDK are of greater importance in stress (Figure 3E, 3F), which suggests that increased CDK-
264 dependent phosphorylation is required to counteract CN-dependent dephosphorylation. Finally,
265 cells expressing the Hcm1-3N protein, which has increased activity because it is stabilized but
266 retains phosphorylation-dependent activation[18], confers a fitness advantage in LiCl stress (Figure
267 4C). Together, these data demonstrate that Hcm1 activity is required for fitness in stress, and that
268 its dynamic phosphoregulation is critical.

269 Dynamic regulation is a recognized feature of many TFs, most notably TFs that respond
270 to stress. In mammalian cells pulsatile nuclear localization and activation of NFAT[25], p53[26–28] and
271 NFκB[29–32] lead to an altered transcriptional output in response to different signals. In budding
272 yeast, at least ten TFs display pulsatile nuclear localization in response to specific cues, thereby
273 increasing frequency of their activation[33]. In the case of the stress-activated TF Msn2, exposure
274 to distinct stressors triggers either sustained or pulsatile Msn2 nuclear localization[34], resulting in
275 expression of distinct groups of target genes belonging to different promoter classes[23,24]. Notably,
276 the CN-regulated TF Crz1 also exhibits pulsative activation via regulation of its nuclear
277 localization[21,22]. When cells are exposed to continuous extracellular $CaCl_2$, the frequency of
278 cytosolic Ca^{2+} pulses increases, and these are followed by pulses of CN activation. CN then
279 dephosphorylates Crz1, leading to pulses of nuclear localization and target gene activation.
280 Importantly, Hcm1 does not display pulses of nuclear localization[33], instead its activation is
281 controlled by phosphorylation. Since Hcm1 is also a CN target, we propose that when cells are
282 growing in LiCl stress pulses of CN activity result in dephosphorylation and inactivation of Hcm1,
283 which are then countered by CDK-dependent phosphorylation, leading to pulses of Hcm1 activity.
284 To our knowledge the only described mechanism of TF frequency modulation is through changing

285 TF localization, therefore dynamic phosphorylation represents a novel mechanism of controlling
286 TF target gene expression in stress.

287 Dynamic phosphoregulation is likely to also control the activities of other CDK target
288 proteins in stress. In addition to CN, which antagonizes CDK as well as other kinases[11], the cell
289 cycle-regulatory phosphatase Cdc14 is activated during the stress response[35–37] and could
290 regulate phosphorylation dynamics. Moreover, a recent phosphoproteomic study monitored
291 proteome-wide phosphorylation after acute exposure to more than 100 stress conditions and
292 found that ~20% of phosphorylated proteins show a change in phosphorylation after acute stress
293 exposure[38]. However, monitoring dynamic changes in phosphorylation status has largely been
294 restricted to proteins that undergo a localization change or other easily measurable phenotype.
295 Here, we show that Phosphosite Scanning can be used to reveal the importance of
296 phosphorylation dynamics[18]. Screening mutants in which all sites are mutated to either non-
297 phosphorylatable or phosphomimetic mutations reveals the importance of being able to add and
298 remove phosphates. In addition, by screening mutants that combine phosphosite mutations and
299 wild type sites, Phosphosite Scanning can reveal whether priming sites for the CDK accessory
300 subunit Cks1 are important in stress, supporting the importance of dynamic phosphorylation. We
301 anticipate that this approach will enable the investigation of phosphorylation dynamics of other
302 proteins and reveal whether dynamic phosphorylation is a common mechanism that modulates
303 protein function when cells are growing in stressful environments.
304

305 **Methods**

306 **Yeast strains and plasmids**

307 All cultures were grown in rich medium (YM-1) or synthetic media lacking uracil (C-Ura) with 2%
308 dextrose or galactose. Cultures were grown at 30°C or 23°C as indicated. A record of strains and
309 plasmids used in this study can be found in Tables S1 and S2, respectively.

310

311 **Co-culture competition assays**

312 Pairwise competition assays were done as described in Conti et al. 2023[18]. Strains in which the
313 endogenous copy of *HCM1* is regulated by a galactose inducible promoter (*GAL1p-HCM1*) and
314 expressing either WT or non-fluorescent GFP were transformed with plasmids expressing WT or
315 mutant *HCM1* from the *HCM1* promoter. Initially, cultures were grown in synthetic media lacking
316 uracil with 2% galactose to ensure expression of *HCM1*. Logarithmic phase cells were equally
317 mixed by adding one optical density (OD600) of each strain to the same culture tube in a final
318 volume of 10mL C-Ura with 2% galactose. To determine the starting abundance of each strain,
319 0.15 optical densities were collected from the co-culture tubes. Samples were pelleted by
320 centrifugation, resuspended in 2mL sodium citrate (50mM sodium citrate, 0.02% NaN_3, pH 7.4)
321 and stored at 4°C pending analysis by flow cytometry. To evaluate fitness in LiCl stress, co-
322 cultures were diluted within a range of 0.005-0.04 optical densities (OD_{600}) into synthetic media
323 lacking uracil with 2% dextrose with or without 150mM LiCl after mixing at the start of the
324 experiment. Cultures were then sampled and diluted every 24 hours for a total of 96 hours.
325 Cultures reached saturation prior to dilution. At each timepoint, 0.15 optical densities were
326 collected, pelleted, and resuspended in 2mL sodium citrate, and stored at 4°C until the conclusion
327 of the experiment. Following the final timepoint, the percentage of GFP positive cells was
328 quantified in each sample using a Guava EasyCyte HT flow cytometer and GuavaSoft software.
329 5000 cells were measured in all samples. Results were analyzed using FloJo software. Averages
330 of n=3-13 biological replicates are shown, exact number is indicated in the figure legends.
331 Selection coefficients for pairwise assays were calculated by calculating the slope of the best fit
332 line of log2 fold change in mutant fraction over time, relative to WT in the same experiment.

333

334 **Western blotting**

335 Yeast culture amounting to one optical density (OD600) was collected, pelleted by centrifugation,
336 and stored at -80°C prior to lysis. Cell pellets were lysed by incubation with cold TCA buffer (10mM
337 Tris pH 8.0, 10% trichloroacetic acid, 25mM ammonium acetate, 1mM EDTA) on ice for 10
338 minutes. Lysates were mixed by vortexing and pelleted by centrifugation at 16,000xg for 10
339 minutes at 4°C. The supernatant was aspirated, and cell pellets were resuspended in 75μL
340 resuspension solution (100mM Tris pH 11, 3% SDS). Lysates were incubated at 95°C for five
341 minutes then allowed to cool to room temperature for five minutes. Lysates were clarified by
342 centrifugation at 16,000xg for 30 seconds at room temperature. Supernatants were then collected,
343 transferred to a new tube and 25μL 4X SDS-PAGE sample buffer (250mM Tris pH 6.8, 8% SDS,
344 40% glycerol, 20% β-mercaptoethanol) was added. The samples were incubated at 95°C for five
345 minutes, then allowed to cool to room temperature and stored at -80°C.

346 For standard Western blots, resolving gels contain 10% acrylamide/bis solution 37.5:1,
347 0.375M Tris pH 8.8, 0.1% SDS, 0.1% ammonium persulfate (APS), 0.04%
348 tetremethylethylenediamine (TEMED). Phos-tag gels contain 6% acrylamide/bis solution 29:1,
349 386mM Tris pH 8.8, 0.1% SDS, 0.2% APS, 25μM Phos-tag acrylamide (Wako), 50μM manganese
350 chloride and 0.17% TEMED. All stacking gels contain 5% acrylamide/bis solution 37.5:1, 126mM
351 Tris pH 6.8, 0.1% SDS, 0.1% APS and 0.1% TEMED. All SDS-PAGE gels were run in 1X running
352 buffer (200mM glycine, 25mM Tris, 35mM SDS). Phos-tag gels were washed twice with 1X
353 transfer buffer containing 10mM EDTA for 15 minutes (150mM glycine, 20mM Tris, 1.25mM SDS,
354 20% methanol) and once with 1X transfer buffer for 10 minutes on a shaking platform with gentle
355 agitation. All gels were transferred to nitrocellulose in cold 1X transfer buffer at 0.45A for two
356 hours. After transfer, nitrocellulose membranes were blocked in a 4% milk solution for 30 minutes.

357 Western blotting was performed with primary antibodies that recognize a V5 epitope tag
358 (Invitrogen, 1:1000 dilution) or PSTAIRE (P7962, Sigma, 1:10,000 dilution). Primary antibody
359 incubations were done overnight at 4°C. Importantly, molecular weight makers are not shown with
360 Phos-tag gels as they do not accurately reflect the molecular weight of proteins.

361

362 **Phosphosite Scanning screens**

363 Phosphosite scanning screens were carried out using pooled plasmid libraries that had been
364 previously constructed[18] and transformed into a *GAL1p-HCM1* strain. A plasmid expressing WT
365 *HCM1* was added to all libraries as a control. During transformation, cells were cultured in YM-1
366 containing 2% galactose to maintain expression of endogenous *HCM1.* Following transformation,
367 cells were cultured overnight at 23°C in synthetic media lacking uracil (C-Ura) with 2% galactose.
368 After approximately 16 hours, an aliquot of transformed cells was removed and plated on C-Ura
369 to confirm a transformation efficiency of at least 10X library size. Remaining cells were washed
370 with 15mL C-Ura with 2% galactose five times, resuspended in 50mL C-Ura with 2% galactose
371 and allowed to grow to logarithmic phase for approximately 48 hours at 30°C. The starting
372 population was sampled to determine the initial abundance of each mutant in the population prior
373 to selection. Cell pellets amounting to 20 optical densities were harvested, frozen on dry ice, and
374 stored at -80°C prior to preparation of sequencing libraries. To evaluate fitness in stress, cultures
375 were then diluted into synthetic media lacking uracil with 2% dextrose with or without 150mM LiCl
376 after sampling at time zero. For all timepoints after time zero, cells were diluted into a range of
377 0.08 and 0.1 optical densities in 10mL of the appropriate media. At each timepoint, cultures
378 reached saturation prior to sampling and dilution. Cultures were sampled and diluted as above
379 every 24 hours for a total of 72 hours.

380

381 **Illumina sequencing library preps**

382 For analysis by sequencing, plasmids were recovered from the frozen samples using a YeaStar
383 Genomic DNA Kit (Zymo Research). Mutant *hcm1* sequence was amplified by PCR (21 cycles)
384 using plasmid specific primers and Phusion High-Fidelity DNA polymerase (New England Biolabs).
385 DNA fragments were purified from a 1% agarose gel using a QIAquick Gel Extraction Kit (Qiagen).
386 Barcoded TruSeq adapters were added to the mutant fragments by PCR (7 cycles) using primers
387 specific to the *HCM1* region fused to either the TruSeq universal adapter or to a unique TruSeq
388 indexed adapter. Sequences of oligonucleotides that were used in library construction can be
389 found in Table S3. Barcoded fragments were purified from a 1% agarose gel as described above.
390 Pooled barcoded libraries were sequenced on a HiSeq4000 platform (Novogene) to obtain paired-
391 end 150 base pair sequencing reads. All sequencing data is available from the NCBI Sequencing
392 Read Archive under BioProject # PRJNA1117860.

393

394 **Phosphosite scanning data analysis**

395 Abundance of *HCM1* alleles was quantified by counting all paired-end sequencing fragments that
396 had an exact match to an expected sequence in both reads using a custom python script. Custom
397 scripts used to generate count tables are available on GitHub
398 (https://github.com/radio1988/mutcount2024/tree/main/AE_type) and Zenodo
399 (https://zenodo.org/records/13144766). Selection coefficients were calculated as the slope of the
400 log2 fraction of reads versus time for each mutant, normalized to the log2 fraction of reads versus
401 time of WT. All selection coefficients for all screens can be found in Dataset S1. Box and whisker
402 plots were generated using GraphPad Prism software. In all box and whisker plots the black
403 center line indicates the median selection coefficient, boxes indicate the 25th-75th percentiles,

404 black lines represent 1.5 interquartile range (IQR) of the 25th and 75th percentile, black circles
405 represent outliers.

406

407 **RNA purification**

408 Cells amounting to five optical densities were harvested, pelleted by centrifugation at 3000rpm
409 for three minutes, and stored at -80°C. Cell pellets were then thawed on ice, resuspended in
410 400μL AE buffer (50mM sodium acetate pH 5.3, 10mM EDTA), and moved to room temperature.
411 40μL 10% SDS and 400μL AE equilibrated phenol was added to each sample and thoroughly
412 mixed by vortexing for 30 seconds. Samples were heated to 65°C for eight minutes and frozen in
413 a dry ice and ethanol bath for five minutes. Organic and aqueous layers were separated by
414 centrifugation at max speed for eight minutes at room temperature. The aqueous layer was then
415 transferred to a new tube. To remove any residual phenol, 500μL phenol:chloroform:isoamyl
416 alcohol was added and thoroughly mixed by vortexing for 30 seconds. Samples were incubated
417 at room temperature for five minutes and the aqueous and organic layers were separated by
418 centrifugation at maximum speed for five minutes at room temperature. The aqueous layer was
419 transferred to a new tube (~450μL) and the nucleic acids were precipitated by adding 40μL 3M
420 NaOAc pH 5.2 and 1mL 100% ethanol. Samples were mixed by vortexing for 15 seconds and
421 frozen in a dry ice and ethanol bath until completely frozen. Samples were then centrifuged at
422 maximum speed for 10 minutes at 4°C. Supernatants were decanted and pellets washed with 80%
423 ethanol and centrifuged at maximum speed for two minutes at 4°C. Supernatants were removed,
424 pellets allowed to dry completely and resuspended in 50μL water. DNA was degraded by
425 treatment with DNaseI. Samples were transferred to PCR strip tubes, 10μL 10X DNaseI buffer,
426 2μL DNaseI and 38μL water was added to each sample, and the samples were mixed by vortexing.
427 Samples were incubated at 30°C for 30 minutes, then cooled to 4°C in a thermocycler. 1μL 0.5M

428 EDTA was added to each sample and mixed. Samples were then heated to 75°C for 10 minutes
429 and cooled to 4°C in a thermocycler. Purified RNA (100μL) was then transferred to a new tube
430 and precipitated by adding 10μL sodium acetate pH 5.2 and 250μL 100% ethanol, and frozen in
431 a dry ice and ethanol bath until completely frozen. RNA was then pelleted by centrifugation at
432 maximum speed for 15 minutes at 4°C. Supernatants were decanted, the pellets washed with 80%
433 ethanol, centrifuged at maximum speed for 2 minutes at 4°C. Supernatants were decanted and
434 pellets allowed to air dry. Pure RNA was resuspended in water. Three biological replicates were
435 performed. Library preparation and sequencing, including polyA mRNA selection, strand specific
436 library preparation, and paired-end 100 base pair sequencing, were performed by Innomics/BGI
437 Americas. All sequencing data is available in NCBI GEO and is accessible through GEO
438 accession number GSE276435.

439

440 **RNAseq analysis**

441 RNASeq analysis was performed with OneStopRNAseq[39]. Paired-end reads were aligned to
442 Saccharomyces_cerevisiae.R64-1-1, with 2.7.7a[40], and annotated with
443 Saccharomyces_cerevisiae.R64-1-1.90.gtf. Aligned exon fragments with mapping quality higher
444 than 20 were counted toward gene expression with featureCounts[41]. Differential expression (DE)
445 analysis was performed with DESeq2[42]. Within DE analysis, 'ashr' was used to create log2 Fold
446 Change (LFC) shrinkage [43] for all possible comparisons of WT and mutant strains, in both control
447 and LiCl conditions. Significant DE genes (DEGs) were filtered with the criteria FDR < 0.05. Gene
448 set enrichment analysis was performed for Hcm1 targets genes using GSEA[44] on the ranked LFC.
449 GSEA results are included in Dataset S2.

450

451 **Flow cytometry**

452 To analyze DNA content by flow cytometry, cells amounting to 0.15 optical densities were collected,
453 fixed in 70% ethanol and stored at 4°C. Cells were then pelleted by centrifugation at 3000rpm for
454 three minutes, resuspended in 1mL sodium citrate buffer (50mM sodium citrate, 0.02% NaN_3, pH
455 7.4) and sonicated. Samples were then pelleted by centrifugation, resuspended in 1mL sodium
456 citrate buffer containing 0.25mg/mL RNaseA, and incubated at 50°C for one hour. 12.5μL
457 10mg/mL Proteinase K was added to each tube and samples were incubated for an additional
458 hour at 50°C. Following incubation, 1mL sodium citrate buffer containing 0.4μL Sytox green was
459 added to each sample and samples were left at room temperature for 1 hour or 4°C overnight,
460 protected from light, for staining. DNA content was analyzed on a Guava EasyCyte HT flow
461 cytometer and GuavaSoft software. 5000 cells were measured in all samples. Results were
462 analyzed using FloJo software.

463

464 **Acknowledgements**

465 The authors thank Tom Fazzio and members of the Benanti lab for insightful discussions and
466 critical reading of the manuscript. This work was supported by National Institutes of Health grant
467 R35GM136280 to J.A.B.

468

469 **References**

470 1. Senft, D., and Ronai, Z.A. (2016). Adaptive Stress Responses During Tumor Metastasis and
471 Dormancy. Trends Cancer *2*, 429–442. https://doi.org/10.1016/j.trecan.2016.06.004.

472 2. Park, H.-S., Lee, S.C., Cardenas, M.E., and Heitman, J. (2019). Calcium-Calmodulin-
473 Calcineurin Signaling: A Globally Conserved Virulence Cascade in Eukaryotic Microbial
474 Pathogens. Cell Host Microbe *26*, 453–462. https://doi.org/10.1016/j.chom.2019.08.004.

475 3. Gasch, A.P., Spellman, P.T., Kao, C.M., Carmel-Harel, O., Eisen, M.B., Storz, G., Botstein,
476 D., and Brown, P.O. (2000). Genomic Expression Programs in the Response of Yeast Cells to
477 Environmental Changes. Mol. Biol. Cell *11*, 4241–4257. https://doi.org/10.1091/mbc.11.12.4241.

478 4. Causton, H.C., Ren, B., Koh, S.S., Harbison, C.T., Kanin, E., Jennings, E.G., Lee, T.I., True,
479 H.L., Lander, E.S., and Young, R.A. (2001). Remodeling of Yeast Genome Expression in
480 Response to Environmental Changes. Mol. Biol. Cell *12*, 323–337.
481 https://doi.org/10.1091/mbc.12.2.323.

482 5. Yaakov, G., Duch, A., García-Rubio, M., Clotet, J., Jiménez, J., Aguilera, A., and Posas, F.
483 (2009). The stress-activated protein kinase Hog1 mediates S phase delay in response to
484 osmostress. Molecular biology of the cell *20*, 3572–3582. https://doi.org/10.1091/mbc.e09-02-
485 0129.

486 6. Clotet, J., Escoté, X., Adrover, M.A., Yaakov, G., Garí, E., Aldea, M., Nadal, E. de, and
487 Posas, F. (2006). Phosphorylation of Hsl1 by Hog1 leads to a G2 arrest essential for cell
488 survival at high osmolarity. EMBO J. *25*, 2338–2346. https://doi.org/10.1038/sj.emboj.7601095.

489 7. Flynn, M.J., Harper, N.W., Li, R., Zhu, L.J., Lee, M.J., and Benanti, J.A. (2024). Calcineurin
490 promotes adaptation to chronic stress through two distinct mechanisms. Mol. Biol. Cell,
491 mbcE24030122. https://doi.org/10.1091/mbc.e24-03-0122.

492 8. Bonny, A.R., Kochanowski, K., Diether, M., and El-Samad, H. (2021). Stress-induced growth
493 rate reduction restricts metabolic resource utilization to modulate osmo-adaptation time. Cell
494 Reports *34*, 108854. https://doi.org/10.1016/j.celrep.2021.108854.

495 9. Ho, Y.-H., Shishkova, E., Hose, J., Coon, J.J., and Gasch, A.P. (2018). Decoupling Yeast
496 Cell Division and Stress Defense Implicates mRNA Repression in Translational Reallocation
497 during Stress. Current Biology *28*, 1–21. https://doi.org/10.1016/j.cub.2018.06.044.

498 10. Cyert, M.S., and Philpott, C.C. (2013). Regulation of cation balance in Saccharomyces
499 cerevisiae. Genetics *193*, 677–713. https://doi.org/10.1534/genetics.112.147207.

500 11. Goldman, A., Roy, J., Bodenmiller, B., Wanka, S., Landry, C.R., Aebersold, R., and Cyert,
501 M.S. (2014). The Calcineurin Signaling Network Evolves via Conserved Kinase-Phosphatase
502 Modules that Transcend Substrate Identity. Mol. Cell.
503 https://doi.org/10.1016/j.molcel.2014.05.012.

504 12. Leech, C.M., Flynn, M.J., Arsenault, H.E., Ou, J., Liu, H., Zhu, L.J., and Benanti, J.A. (2020).
505 The coordinate actions of calcineurin and Hog1 mediate the stress response through multiple
506 nodes of the cell cycle network. PLoS Genetics *16*, e1008600-27.
507 https://doi.org/10.1371/journal.pgen.1008600.

508 13. Arsenault, H.E., Roy, J., Mapa, C.E., Cyert, M.S., and Benanti, J.A. (2015). Hcm1 integrates
509 signals from Cdk1 and Calcineurin to control cell proliferation. Molecular biology of the cell *26*,
510 3570–3577. https://doi.org/10.1091/mbc.e15-07-0469.

511 14. Pramila, T., Wu, W., Miles, S., Noble, W.S., and Breeden, L.L. (2006). The Forkhead
512 transcription factor Hcm1 regulates chromosome segregation genes and fills the S-phase gap in
513 the transcriptional circuitry of the cell cycle. Genes & Development *20*, 2266–2278.
514 https://doi.org/10.1101/gad.1450606.

515 15. Alvarez-Fernández, M., and Medema, R.H. (2013). Novel functions of FoxM1: from
516 molecular mechanisms to cancer therapy. Frontiers in oncology *3*, 30.
517 https://doi.org/10.3389/fonc.2013.00030.

518 16. Landry, B.D., Mapa, C.E., Arsenault, H.E., Poti, K.E., and Benanti, J.A. (2014). Regulation
519 of a transcription factor network by Cdk1 coordinates late cell cycle gene expression. The
520 EMBO Journal *33*, 1044–1060. https://doi.org/10.1002/embj.201386877.

521 17. Flynn, M.J., and Benanti, J.A. (2022). Cip1 tunes cell cycle arrest duration upon calcineurin
522 activation. Proc National Acad Sci *119*, e2202469119.
523 https://doi.org/10.1073/pnas.2202469119.

524 18. Conti, M.M., Li, R., Ramos, M.A.N., Zhu, L.J., Fazzio, T.G., and Benanti, J.A. (2023).
525 Phosphosite Scanning reveals a complex phosphorylation code underlying CDK-dependent
526 activation of Hcm1. Nat Commun *14*, 310. https://doi.org/10.1038/s41467-023-36035-9.

527 19. McGrath, D.A., Balog, E.R.M., Kõivomägi, M., Lucena, R., Mai, M.V., Hirschi, A., Kellogg,
528 D.R., Loog, M., and Rubin, S.M. (2013). Cks confers specificity to phosphorylation-dependent
529 CDK signaling pathways. Nature Structural & Molecular Biology *20*, 1407–1414.
530 https://doi.org/10.1038/nsmb.2707.

531 20. Kõivomägi, M., Örd, M., Iofik, A., Valk, E., Venta, R., Faustova, I., Kivi, R., Balog, E.R.M.,
532 Rubin, S.M., and Loog, M. (2013). Multisite phosphorylation networks as signal processors for
533 Cdk1. Nature Structural & Molecular Biology *20*, 1415–1424. https://doi.org/10.1038/nsmb.2706.

534 21. Hsu, I.S., Strome, B., Plotnikov, S., and Moses, A.M. (2019). A Noisy Analog-to-Digital
535 Converter Connects Cytosolic Calcium Bursts to Transcription Factor Nuclear Localization
536 Pulses in Yeast. G3: Genes, Genomes, Genet. *9*, 561–570.
537 https://doi.org/10.1534/g3.118.200841.

538 22. Cai, L., Dalal, C.K., and Elowitz, M.B. (2008). Frequency-modulated nuclear localization
539 bursts coordinate gene regulation. Nature *455*, 485–490. https://doi.org/10.1038/nature07292.

540 23. Hansen, A.S., and O'Shea, E.K. (2013). Promoter decoding of transcription factor dynamics
541 involves a trade-off between noise and control of gene expression. Mol. Syst. Biol. *9*, 704–704.
542 https://doi.org/10.1038/msb.2013.56.

543 24. Hansen, A.S., and O'Shea, E.K. (2015). Limits on information transduction through
544 amplitude and frequency regulation of transcription factor activity. eLife *4*, e06559.
545 https://doi.org/10.7554/elife.06559.

546 25. Yissachar, N., Sharar Fischler, T., Cohen, A.A., Reich-Zeliger, S., Russ, D., Shifrut, E.,
547 Porat, Z., and Friedman, N. (2013). Dynamic Response Diversity of NFAT Isoforms in Individual
548 Living Cells. Mol. Cell *49*, 322–330. https://doi.org/10.1016/j.molcel.2012.11.003.

549 26. Lahav, G., Rosenfeld, N., Sigal, A., Geva-Zatorsky, N., Levine, A.J., Elowitz, M.B., and Alon,
550 U. (2004). Dynamics of the p53-Mdm2 feedback loop in individual cells. Nat. Genet. *36*, 147–
551 150. https://doi.org/10.1038/ng1293.

552 27. Batchelor, E., Loewer, A., Mock, C., and Lahav, G. (2011). Stimulus-dependent dynamics of
553 p53 in single cells. Mol. Syst. Biol. *7*, 488–488. https://doi.org/10.1038/msb.2011.20.

554 28. Purvis, J.E., Karhohs, K.W., Mock, C., Batchelor, E., Loewer, A., and Lahav, G. (2012). p53
555 dynamics control cell fate. Science (New York, NY) *336*, 1440–1444.
556 https://doi.org/10.1126/science.1218351.

557 29. Lee, T.K., Denny, E.M., Sanghvi, J.C., Gaston, J.E., Maynard, N.D., Hughey, J.J., and
558 Covert, M.W. (2009). A Noisy Paracrine Signal Determines the Cellular NF-κB Response to
559 Lipopolysaccharide. Sci. Signal. *2*, ra65. https://doi.org/10.1126/scisignal.2000599.

560 30. Ashall, L., Horton, C.A., Nelson, D.E., Paszek, P., Harper, C.V., Sillitoe, K., Ryan, S., Spiller,
561 D.G., Unitt, J.F., Broomhead, D.S., et al. (2009). Pulsatile Stimulation Determines Timing and
562 Specificity of NF-κB-Dependent Transcription. Science *324*, 242–246.
563 https://doi.org/10.1126/science.1164860.

564 31. Tay, S., Hughey, J.J., Lee, T.K., Lipniacki, T., Quake, S.R., and Covert, M.W. (2010).
565 Single-cell NF-κB dynamics reveal digital activation and analogue information processing.
566 Nature *466*, 267–271. https://doi.org/10.1038/nature09145.

567 32. Lee, R.E.C., Qasaimeh, M.A., Xia, X., Juncker, D., and Gaudet, S. (2016). NF-κB signalling
568 and cell fate decisions in response to a short pulse of tumour necrosis factor. Sci. Rep. *6*,
569 39519. https://doi.org/10.1038/srep39519.

570 33. Dalal, C.K., Cai, L., Lin, Y., Rahbar, K., and Elowitz, M.B. (2014). Pulsatile dynamics in the
571 yeast proteome. Current biology : CB *24*, 2189–2194. https://doi.org/10.1016/j.cub.2014.07.076.

572 34. Hao, N., and O'Shea, E.K. (2012). Signal-dependent dynamics of transcription factor
573 translocation controls gene expression. Nat. Struct. Mol. Biol. *19*, 31–39.
574 https://doi.org/10.1038/nsmb.2192.

575 35. Reiser, V., D'Aquino, K.E., Ee, L.-S., and Amon, A. (2006). The stress-activated mitogen-
576 activated protein kinase signaling cascade promotes exit from mitosis. Molecular biology of the
577 cell *17*, 3136–3146. https://doi.org/10.1091/mbc.e05-12-1102.

578 36. Chasman, D., Ho, Y.-H., Berry, D.B., Nemec, C.M., MacGilvray, M.E., Hose, J., Merrill, A.E.,
579 Lee, M.V., Will, J.L., Coon, J.J., et al. (2014). Pathway connectivity and signaling coordination in
580 the yeast stress-activated signaling network. Molecular systems biology *10*, 759–759.
581 https://doi.org/10.15252/msb.20145120.

582 37. Tognetti, S., Jiménez, J., Viganò, M., Duch, A., Queralt, E., Nadal, E. de, and Posas, F.
583 (2020). Hog1 activation delays mitotic exit via phosphorylation of Net1. Proceedings of the
584 National Academy of Sciences *1505*, 201918308–201918933.
585 https://doi.org/10.1073/pnas.1918308117.

586 38. Leutert, M., Barente, A.S., Fukuda, N.K., Rodriguez-Mias, R.A., and Villén, J. (2023). The
587 regulatory landscape of the yeast phosphoproteome. Nat. Struct. Mol. Biol. *30*, 1761–1773.
588 https://doi.org/10.1038/s41594-023-01115-3.

589 39. Li, R., Hu, K., Liu, H., Green, M.R., and Zhu, L.J. (2020). OneStopRNAseq: A Web
590 Application for Comprehensive and Efficient Analyses of RNA-Seq Data. Genes-basel *11*, 1165.
591 https://doi.org/10.3390/genes11101165.

592 40. Dobin, A., Davis, C.A., Schlesinger, F., Drenkow, J., Zaleski, C., Jha, S., Batut, P.,
593 Chaisson, M., and Gingeras, T.R. (2013). STAR: ultrafast universal RNA-seq aligner.
594 Bioinformatics *29*, 15–21. https://doi.org/10.1093/bioinformatics/bts635.

595 41. Liao, Y., Smyth, G.K., and Shi, W. (2014). featureCounts: an efficient general purpose
596 program for assigning sequence reads to genomic features. Bioinformatics *30*, 923–930.
597 https://doi.org/10.1093/bioinformatics/btt656.

598 42. Love, M.I., Huber, W., and Anders, S. (2014). Moderated estimation of fold change and
599 dispersion for RNA-seq data with DESeq2. Genome Biol *15*, 550.
600 https://doi.org/10.1186/s13059-014-0550-8.

601 43. Stephens, M. (2017). False discovery rates: a new deal. Biostat Oxf Engl *18*, 275–294.
602 https://doi.org/10.1093/biostatistics/kxw041.

603 44. Subramanian, A., Tamayo, P., Mootha, V.K., Mukherjee, S., Ebert, B.L., Gillette, M.A.,
604 Paulovich, A., Pomeroy, S.L., Golub, T.R., Lander, E.S., et al. (2005). Gene set enrichment
605 analysis: A knowledge-based approach for interpreting genome-wide expression profiles. Proc
606 National Acad Sci *102*, 15545–15550. https://doi.org/10.1073/pnas.0506580102.

607

608 **Figure Legends**

609 **Figure 1. Expression of a phosphomimetic Hcm1 mutant decreases fitness in LiCl stress**

610 (A) Hcm1 activity is regulated by cyclin-dependent kinase (CDK) and the phosphatase calcineurin
611 (CN). (B) Phos-tag and standard Western blots showing Hcm1 phosphorylation and expression
612 after the indicated number of hours in LiCl stress. Hcm1 was detected with an antibody that
613 recognizes a 3V5 tag, PSTAIRE is shown as a loading control. Representative blots from n=3
614 experiments are shown. (C-D) Strains with the indicated genotypes were co-cultured in control
615 media (C) or media with 150mM LiCl (D). Percentage of each strain was quantified by flow
616 cytometry at the indicated timepoints. An average of n=3 biological replicates is shown. Error bars
617 represent standard deviations.

618

619 **Figure 2. Phosphosite mutations in Hcm1 decrease fitness in stress.**

620 (A) Schematic of Phosphosite Scanning screens. Plasmids expressing all 256 mutants in the A/E
621 library, as well as WT *HCM1*, were transformed into a strain in which expression of the genomic
622 copy of *HCM1* is controlled by a galactose-inducible promoter. The pooled population growing in
623 galactose was diluted and split into dextrose containing media (to shut-off expression of the
624 endogenous copy of WT *HCM1*) with or without 150mM LiCl at the start of the experiment. (B)
625 Scatterplot comparing average selection coefficients for each mutant in the A/E library in control
626 and LiCl media. Pearson correlation (r) is indicated. (C-E) Box and whisker plots comparing the
627 selection coefficients of different groups of mutants. The black center line indicates the median
628 selection coefficient, boxes indicate the 25th-75th percentiles, whiskers represent 1.5 interquartile
629 range (IQR) of the 25th and 75th percentile, black circles represent outliers. In all panels, selection
630 coefficients are an average of n=4 biological replicates. (C) shows selection coefficients in cells
631 with the indicated number of phosphomimetic mutations in control or LiCl conditions. (D-E) show
632 selection coefficients of mutants that are either phosphodead or phosphomimetic at each position,
633 in control (D) or LiCl containing medium (E).

634

635 **Figure 3. Elevated importance of processive Hcm1 phosphorylation in stress**

636 (A) Scatterplot comparing average selection coefficients for each mutant in the W/E library in
637 control and LiCl media. Pearson correlation (r) is indicated. Red represents mutants that are
638 phosphomimetic at sites T460 and S471, blue represents all other mutants. (B-F) Box and whisker
639 plots comparing the selection coefficients of different groups of mutants. The black center line
640 indicates the median selection coefficient, boxes indicate the 25th-75th percentiles, whiskers
641 represent 1.5 interquartile range (IQR) of the 25th and 75th percentile, black circles represent
642 outliers. In all panels, selection coefficients are an average of n=4 biological replicates. (B) shows
643 selection coefficients in cells with the indicated number of phosphomimetic mutations in control

644 or LiCl conditions. (C-D) show selection coefficients of mutants that are either WT (S or T) or
645 phosphomimetic at each position, in control (C) or LiCl containing medium (D). (E-F) show
646 selection coefficients for mutants that are WT (TT) or phosphomimetic (EE) at indicated positions.

647

648 **Figure 4. Dynamic phosphorylation of the Hcm1 TAD promotes fitness in stress.**

649 (A) Diagram of Hcm1 mutant proteins showing mutated phosphosites and impacts on protein
650 stability and phosphoregulation of the TAD region. nc, no change. (B-E) Strains with the indicated
651 genotypes were co-cultured in control media (B, D) or media with 150mM LiCl (C, E). Percentage
652 of each strain was quantified by flow cytometry at the indicated timepoints. An average of n=13
653 biological replicates is shown. Error bars represent standard deviations. (F) Comparison of
654 selection coefficients of the indicated strains and growth conditions, from pairwise assays shown
655 in Figures 1C, 1D, 4B, and 4C. One-way ordinary ANOVA with Šídák's multiple comparisons test
656 was used to test significance, *$p<0.0001$. (G) Normalized enrichment scores (NES) of Hcm1
657 target genes from GSEA analysis of the indicated comparisons. Asterisk (*) indicates FDR=0.

658

Figure 1

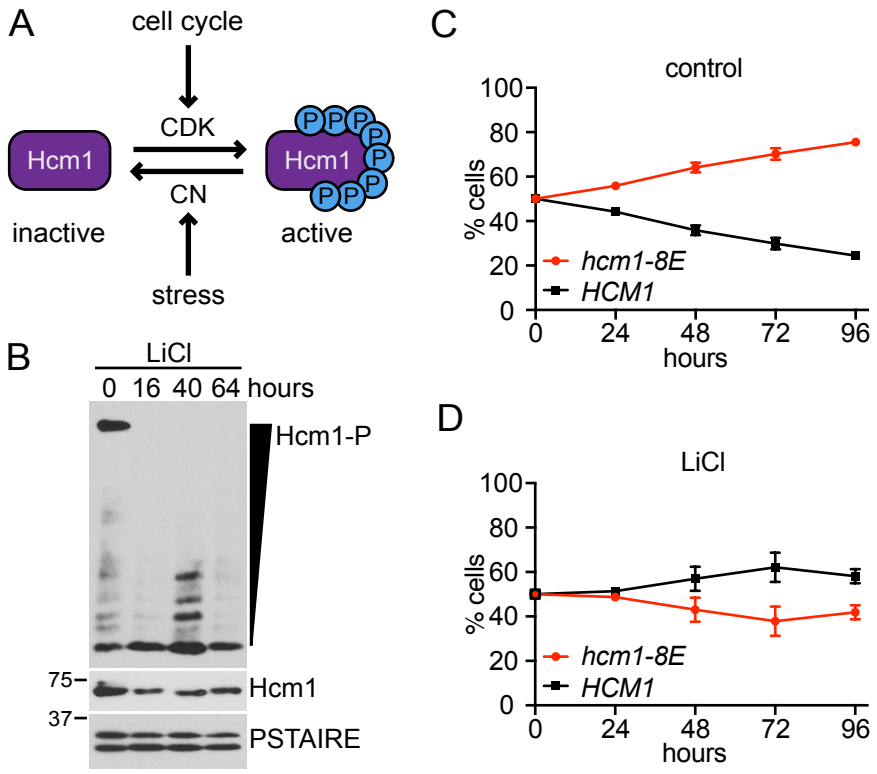
A
cell cycle
CDK
Hcm1
Hcm1
P
CN
inactive
active
stress
B
LiCl
0 16 40 64 hours
Hcm1-P
75
Hcm1
37
PSTAIRE
C
control
100
80
60
40
20
0
% cells
hcm1-8E
HCM1
0 24 48 72 96
hours
D
LiCl
100
80
60
40
20
0
% cells
hcm1-8E
HCM1
0 24 48 72 96
hours

Figure 2

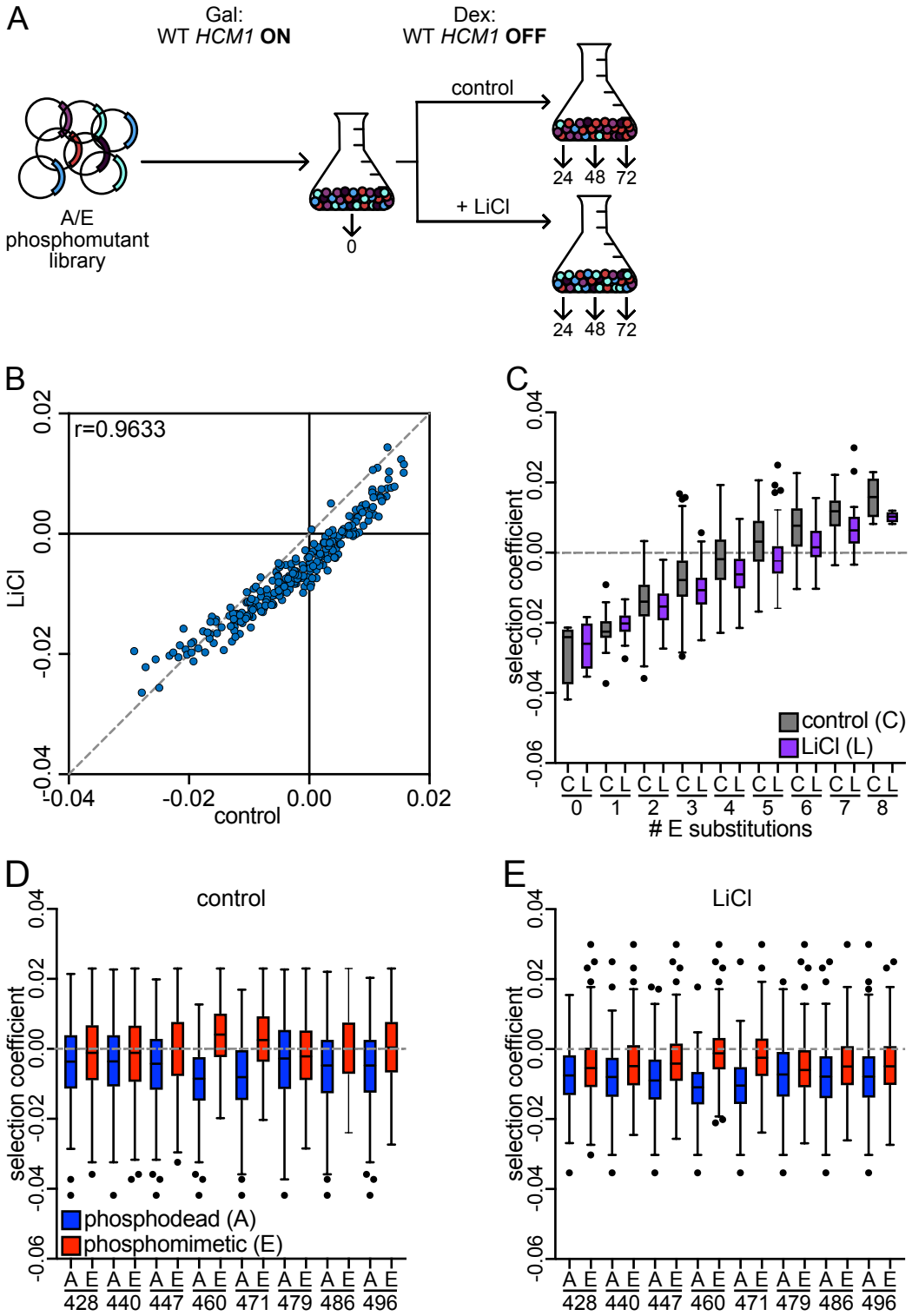
A
Gal:
WT HCM1 ON
Dex:
WT HCM1 OFF
control
+ LiCl
A/E
phosphomutant
library
0
24 48 72
24 48 72
B
r=0.9633
LiCl
control
C
selection coefficient
control (C)
LiCl (L)
E substitutions
D
control
selection coefficient
phosphodead (A)
phosphomimetic (E)
E
LiCl
selection coefficient

Figure 3

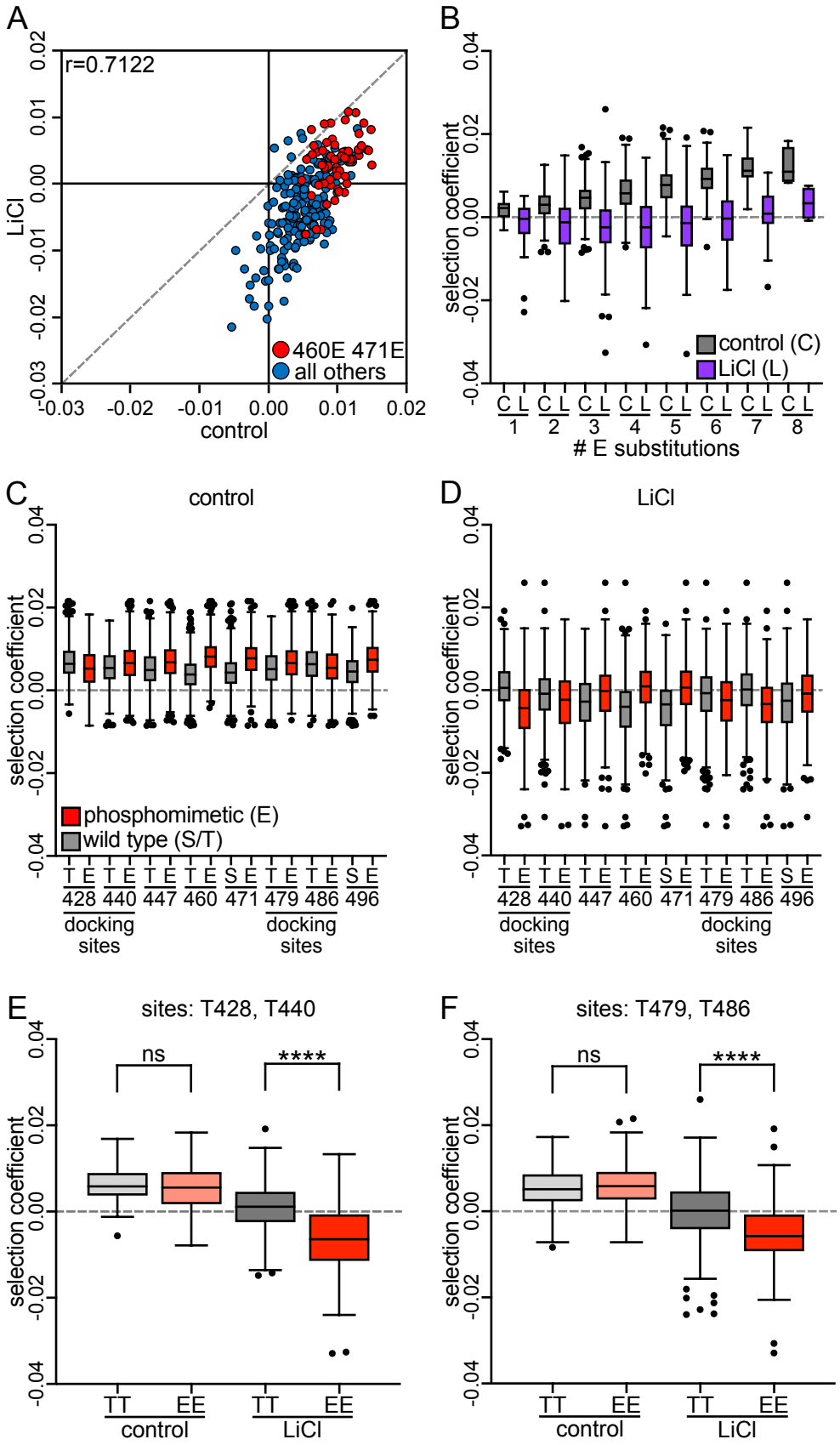
A
r=0.7122
LiCl
control
460E 471E
all others
B
selection coefficient
control (C)
LiCl (L)
E substitutions
C
control
selection coefficient
phosphomimetic (E)
wild type (S/T)
docking sites
D
LiCl
E
sites: T428, T440
ns
****
TT
EE
control
LiCl
F
sites: T479, T486

Figure 4

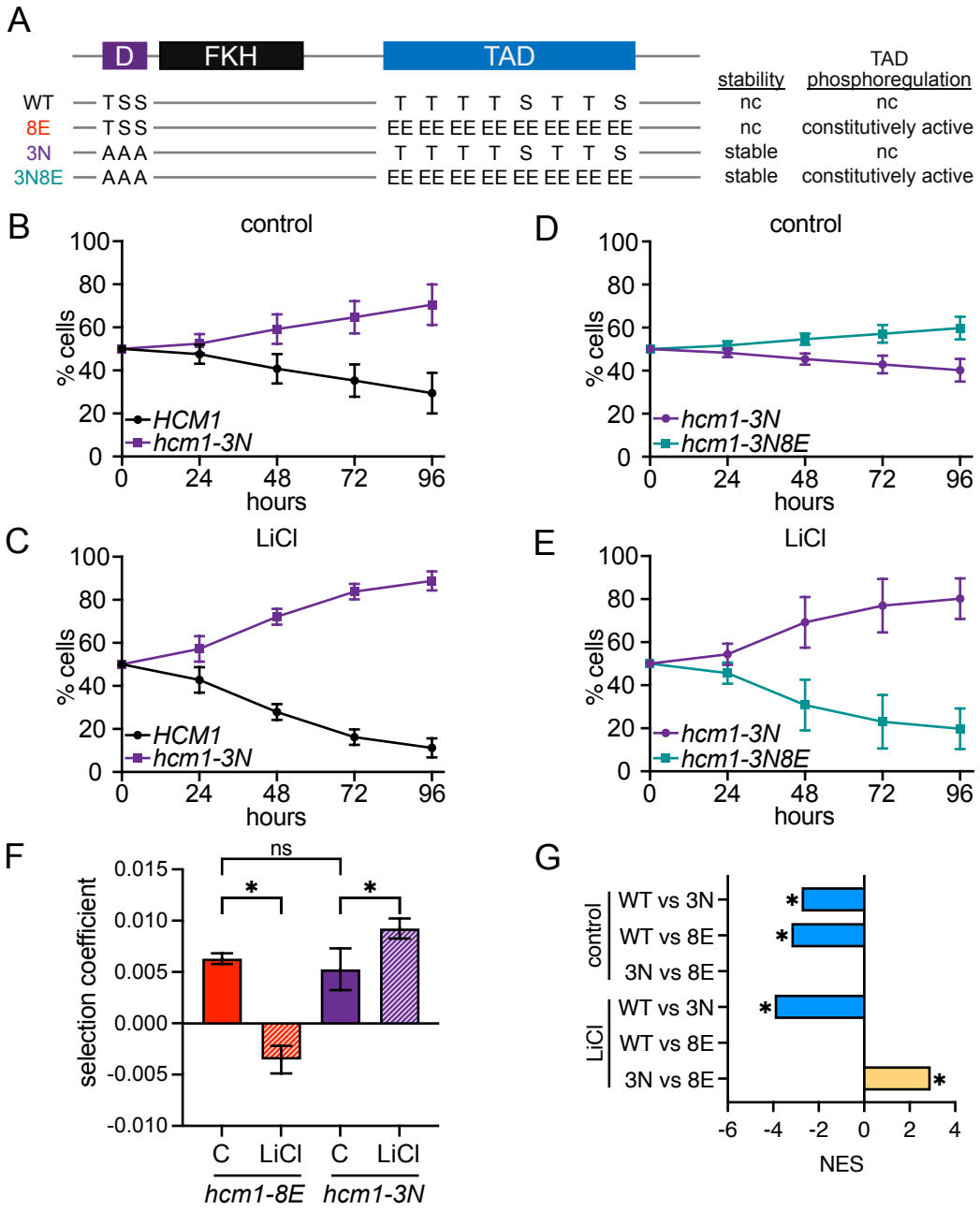
A
D
FKH
TAD
stability
TAD phosphoregulation
WT TSS T T T T S T T S nc nc
8E TSS EE EE EE EE EE EE EE EE nc constitutively active
3N AAA T T T T S T T S stable nc
3N8E AAA EE EE EE EE EE EE EE EE stable constitutively active
B
control
% cells
HCM1
hcm1-3N
hours
C
LiCl
D
hcm1-3N8E
E
F
ns
selection coefficient
C
LiCl
hcm1-8E
hcm1-3N
G
WT vs 3N
WT vs 8E
3N vs 8E
control
LiCl
NES